$AAg_2M[VO_4]_2$ (A = Ba, Sr; M = Co, Ni): A series of ferromagnetic insulators

Angela Möller,[1,*] Ngozi E. Amuneke,[1] Phillip Daniel,[1] Bernd Lorenz,[2] Clarina R. de la Cruz,[3] Melissa Gooch,[2] and Paul C. W. Chu[2]

[1]*Texas Center for Superconductivity and Department of Chemistry, University of Houston, Houston, Texas 77204-5003, USA*

[2]*Texas Center for Superconductivity and Department of Physics, University of Houston, Houston, Texas 77204-5005, USA*

[3]*7 QCMD, Neutron Sciences Directorate, Oak Ridge National Laboratory, Oak Ridge, Tennessee 38831, USA*

(Received 15 March 2012; revised manuscript received 5 June 2012; published 20 June 2012)

$AAg_2M[VO_4]_2$ with $A = Sr^{2+}$ or Ba^{2+} present a series of layered compounds featuring a triangular lattice of transition metal cations, $M = Co^{2+}$ or Ni^{2+}, connected via nonmagnetic ortho-vanadates, which provide the magnetic superexchange within the layers. For this series of insulating compounds, ferromagnetic long-range order below 10 K is suggested by magnetization and specific heat measurements and confirmed by neutron diffraction experiments. We have investigated the impact of the spacer size of A^{2+} separating the layers leading to a tilting of the vanadates and consequently inducing a change in the effective magnetic correlations. Magnetization and specific heat measurements corroborate the important dependence of the magnetic superexchange on the orientation of the vanadates and the respective spin system. Furthermore, the ground state properties of the spin systems, $S = 1$ (Ni^{2+}) and $S = 3/2$ (Co^{2+}) in their respective octahedral coordination of oxygen, are evaluated. Calculated magnetic moments of the single ion complexes agree well with the magnetic structure. We, furthermore, report the dependence of T_c on applied isotropic pressure suggestive of a pressure effect on the effective ferromagnetic exchange coupling constants. In addition spectroscopic investigations probing the electronic structure of the $[MO_6]$ complexes and the vibrational structure of the $[VO_4]$ units are given.

DOI: 10.1103/PhysRevB.85.214422 PACS number(s): 75.50.Dd, 61.05.fm, 82.33.Pt

I. INTRODUCTION

Structure-property relationships have fascinated solid state scientists for decades and interdisciplinary research to study the interplay of various degrees of freedom in highly correlated electron systems are still an on-going demanding issue. In particular, the diversity of ground states low-dimensional and even more so geometrically frustrated systems may exhibit, give rise to fascinating phenomena.[1–6] For systems representative of low-dimensional magnetic interactions of small spins and geometrical frustration, the macroscopic properties are generally strongly affected by quantum fluctuations. Here, the two-dimensional cases, the triangular or the kagomé lattice, have been identified as suitable candidates.[3,7] They all contain the motif of a triangle as the main structural feature leading to degenerate ground states. Thus it is critical not to remove this degeneracy by a structural distortion, which will eventually lead toward classical ground states. Typical for real systems, an anisotropy of the magnetic exchange may also be introduced by the splitting of the single ion ground state through spin-orbit coupling.[8–10]

Therefore it remains an interesting challenge for preparative chemists to identify new classes of model materials. Experimentally studied examples of the frustrated 2D cases are scarce with prominent, intriguing compounds such as $NiGa_2S_4$,[11] $RbFe[MoO_4]_2$,[12–14] $CuFeO_2$,[15] or $AM_3(OH)_6(SO_4)_2$—the jarosite type of compounds.[16–18] Here, we present a class of materials where a reduction of the dimensionality of a system can be achieved by using "chemical scissors," such as nonmagnetic large counter ions (e.g., A^{2+} = Sr or Ba), see Fig. 1. Another aspect to preserve geometric frustrated structural motifs, here on the triangular lattice, include building blocks with a threefold symmetry (e.g., T_d, C_{3v}, or D_{3h}) to link the magnetic cations. Thereby, the magnetic exchange will involve superexchange via a nonmagnetic complex anion, $[VO_4]^{3-}$ (see Fig. 2), which eventually will involve empty d-orbitals mixing in and presents an interesting opportunity of tuning magnetic couplings through the relative orientation of the tetrahedral versus the octahedral units. An intriguing scenario arises for the effective magnetic coupling, if the V d-orbital mediated exchange couplings are of opposite sign compared with the more common M/O$\cdots$O/M exchange pathway.[19] This may lead to counterintuitive results originating from the presence of ferromagnetic (FM) and antiferromagnetic (AFM) coupled $S = 1/2$ chains, as was recently discussed for $BaAg_2Cu[VO_4]_2$.[20,21]

These considerations have motivated us to target a 2D model system with the motif of a triangular lattice of magnetic $3d$ transition metal ions exclusively bridged by nonmagnetic linkers, $AAg_2M[VO_4]_2$, with A^{2+} = Sr or Ba and M^{2+} = Co, Ni, Mg. The two former transition metal ions are magnetic and represent the spin systems of $S = 3/2$ and 1, respectively. For these cases, we find materials that belong to a scarce class of ferromagnetic (FM) insulators as indicated by spectroscopic measurements. The scope of this work is to reveal the importance of the superexchange coupling (d_M-p_O-d_V-p_O-d_M pathways) depending on so-called chemical (anisotropic) and physical (isotropic) pressures. We will show that the magnetic couplings are quite sensitive to the rather small imposed structural distortions. Furthermore, it is important to consider the differences in the single-ion anisotropy introduced through spin-orbit coupling occurring at similar temperatures as the magnetic order here. Hence, we anticipate the realization of different theoretical models, such as the Heisenberg or Ising model, for these spin systems on the triangular lattice. An interesting aspect is that for a 2D-FM spin system the ground state remains degenerate by symmetry whereas frustration phenomena will arise, e.g., from one of the three equal and effectively FM exchange coupling constants tuned into the

 ©2012 American Physical Society

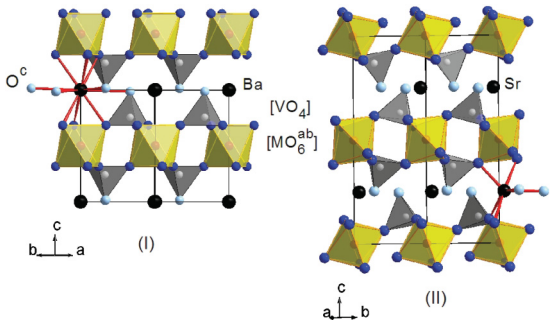

FIG. 1. (Color online) Projection of the crystal structures of the $BaAg_2M[VO_4]_2$ (left) and $SrAg_2M[VO_4]_2$ (right), denoted structure type (I) and (II), respectively. Reference to O^{ab} (dark blue) and O^c (bright blue) are included. For simplicity, the Ag atoms are not depicted. The coordination spheres of the A cations are shown (red bonds).

AFM regime. Recently, frustrated FM lattices have emerged as an intriguing topic in condensed matter theory,[22–27] and we believe that our series of compounds may prove suitable for further development of new insights into the competition of various degrees of freedom.

The manuscript is organized as follows. First, we will discuss the major structural features in the context of probing the impact of the spacer (chemical pressure) on the linker (vanadate). The spectroscopic work aims at characterizing the single ion complexes with the ligand field calculations providing a reference for the paramagnetic properties. The measured thermodynamic properties will allow insights into the respective models being realized here. The evaluation will be completed through neutron diffraction data confirming the respective magnetic structures.

II. METHODS

Powder samples of $AAg_2M[VO_4]_2$ were prepared by solid-state techniques from ACO_3 (A = Sr, Ba), MCO_3 (M = Co, Ni) or $4MgCO_3{\cdot}Mg(OH)_2{\cdot}4H_2O$, respectively, and $AgVO_3$ (obtained from reacting Ag_2O and V_2O_5 at 753 K) in stoichiometric ratios. The starting materials were ground, pressed in pellets, and reacted in corundum crucibles in air. Typical reaction conditions involved initial heating at 823 K for 3 days. Then the samples were reground, pelletized, and annealed again between 853 to 873 K for 5 days. The phase purity of the compounds were verified by x-ray diffraction (X'Pert Pro PANanalytical) using Cu radiation. Lattice constants were derived from LeBail fits using the program package FULLPROF.[28] Spectroscopic measurements were carried out at room temperature in reflectance mode in the mid-infrared (MIR, 400−4000 cm^{-1}) and ultraviolet to near-infrared (UV-vis-NIR, 5000−35000 cm^{-1}) light using a Bruker Alpha-P FT and a Varian Cary500 instrument, respectively. Magnetic susceptibilities were measured with a magnetic properties measurement system (MPMS) and a physical properties measurement system (PPMS) in the temperature range 2−300 K in applied fields up to 0.1 T (zero field and field cooled). The field-dependent magnetization measurements were carried out between 2−15 K. Specific heat measurements (PPMS) were performed in zero-field and applied fields up to 5 T. To investigate the physical pressure effect on the magnetic phase transitions, the ac magnetic susceptibility was measured through a dual coil system attached to the samples by recording the mutual inductance signal employing the LR700 (Linear Research) resistance/inductance bridge. Pressure up to 1.9 GPa was generated in a piston-cylinder high-pressure clamp cell. The sample was mounted in a Teflon container and a 1 : 1 mixture of Fluorinert FC70 and FC77 was used as a pressure transmitting medium. Temperature was controlled between ambient and 1.2 K by inserting the pressure cell into a liquid helium dewar. The pressure was determined *in situ* at low temperatures by measuring the shift of the superconducting transition of high-purity lead. Neutron diffraction measurements were done at the HB-2A high-resolution powder diffractometer at the High Flux Isotope Reactor at Oak Ridge National Laboratory. A wavelength of $\lambda = 2.408$ Å was used with a Ge(113) monochromator and 12′-31′-6′ collimation. Diffraction patterns of the samples inside the aluminum containers were measured between 60 and 2 K using a liquid helium cryostat.

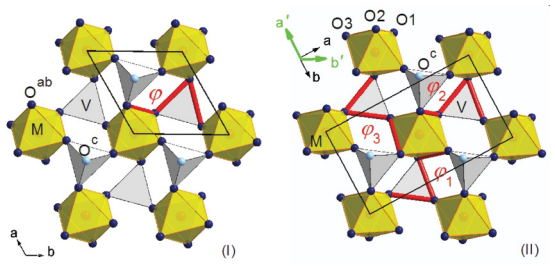

FIG. 2. (Color online) Triangular lattices of magnetic ions bridged via nonmagnetic vanadates in $BaAg_2M[VO_4]_2$ (left) and $SrAg_2M[VO_4]_2$ (right). To facilitate reference to the triangular lattice we will transform the unit cell (II) into a pseudohexagonal setting with lattice constants a' and b' (green reference system). The orientation of the vanadates (grey) with respect to the $[MO_6]$ octahedra (yellow) along the a and b axis and the diagonal direction in the ab plane can be quantified by the dihedral angles, φ (red), respectively (see text for details).

III. CRYSTAL STRUCTURE

$BaAg_2M[VO_4]_2$ (I) and $SrAg_2M[VO_4]_2$ (II) with M^{2+} = Co, Ni, or Mg present new members of a series of compounds that crystallize isotypic to the respective $AAg_2Mn[VO_4]_2$ type of structures with A^{2+} = Ba (I) or Sr (II) reported by Müller-Buschbaum.[29,30] A detailed description of the structural features are given there and see also Ref. 20 for the neglected discussion of the Ag coordination and connectivity. Both structure types (see Figs. 1 and 2) are layered with the A^{2+} cations representing the spacer. The magnetic transition metal cations, M^{2+} are arranged on a planar triangular lattice, $d(M-M) \approx 5.53$ Å and bridged via the three basal O^{ab} of the complex nonmagnetic $[VO_4]^{3-}$. These bridging groups are centering each (M_3) triangle in an alternating fashion above and below each layer (see Fig. 2). The Ag^+ ions (not shown here) complement the two-dimensional feature by filling the remaining voids left unoccupied by the vanadates. The two type of structures (see Fig. 1) are closely related. Whereas for

TABLE I. Interatomic distances (in Å) and angles (in degrees) for the $BaAg_2M[VO_4]_2$ (I) and $SrAg_2M[VO_4]_2$ (II) type of structures with A = Ba or Sr and M = Co or Ni, respectively, see Fig. 1 and text for details. Reference to the crystallographic axis are abbreviated to the pseudo-hexagonal settings for the triangular lattice for (II): a' and b'. The distances to O^{ab} for (II) are listed in the order (O1, O2, O3). The dihedral angles, φ (see Fig. 2) are given for (II) from left to right: φ_1, φ_2, and φ_3.

	(I)	(II)		
M = Co				
A–O^c	6 × 3.195	2 × 2.660		
A–O^{ab}	6 × 2.821	2 × 2.642	2 × 2.523	
V–O^{ab}	3 × 1.713	1.721	1.714	1.704
V–O^c	1.640	1.668		
(Co–Co)^c	7.176	6.866		
(Co–Co)^{ab}	6 × 5.531	2 × 5.596$^{a'}$	2 × 5.565$^{b'}$	2 × 5.596$^{a'b'}$
Co–O^{ab}	6 × 2.129	2 × 2.083	2 × 2.111	2 × 2.178
M = Ni				
A–O^c	6 × 3.182	2 × 2.636		
A–O^{ab}	6 × 2.810	2 × 2.620	2 × 2.524	
V–O^{ab}	3 × 1.706	1.701	1.699	1.692
V–O^c	1.634	1.666		
(Ni–Ni)^c	7.148	6.882		
(Ni–Ni)^{ab}	6 × 5.508	2 × 5.526$^{a'}$	2 × 5.530$^{b'}$	2 × 5.526$^{a'b'}$
Ni–O^{ab}	6 × 2.122	2 × 2.073	2 × 2.098	2 × 2.158
φ	119	147	95	130
$\angle(M$–V–$M)$	97	97$^{a'}$	96$^{b'}$	102$^{a'b'}$

(I) only one almost undistorted layer is present (space group $P\bar{3}$, $Z = 1$) type (II) is a distortion variant (space group $C2/c$, $Z = 4$) for which the layer stacking sequence along the c axis is doubled (two relative orientations occur), $c^{(II)} = 2\,c^{(I)}$. In order to facilitate the description and allow for the discussion of subtle differences of the underlying triangular lattice, we choose to relate (II) to a pseudohexagonal setting in the ab plane and define the new reference as $a' = [0\ -1\ 0]^{(II)}$ and $b' = [\frac{1}{2}\ \frac{1}{2}\ 0]^{(II)}$, see Fig. 2. The main aspects of the structural features are summarized in Table I. The lattice constants[31] have been refined from the experimental x-ray diffraction data shown in Fig. 3.

First, we will discuss structural aspects in relation to the spacer, A^{2+}. Calculations of the Madelung part of the lattice energies (MAPLE)[32,33] allow us to determine the mean effective ionic radii (MEFIR)[34] and the effective coordination numbers (ECoN) for the cations with respect to the ionic radius of O^{2-} of 1.40 Å. The calculated ionic radii of the transition metal cations are as well in line with the respective values given by Shannon.[35] ECoN values of 10 (naive coordination number, C.N. 6 + 6) for Ba^{2+} and seven (naive C.N. 6 + 2) for Sr^{2+} are indicative for the observed structural distortion imposed by the drastic change in ionic radii of the spacer (A^{2+}) from 1.50 Å (I) to 1.23 Å (II). Note, the reduction of the lattice parameter c. In Fig. 1, the respective coordination of Ba^{2+} and Sr^{2+} is depicted and shows the principal effect on the tilting of the vanadates in (II) off the c axis. In (I), all $[VO_4]^{3-}$ units possess C_{3v} symmetry and C_1 in (II) with the shortest V–O^c distance along the c axis. The lower C.N. of Sr^{2+} in (II) leaves one O^{2-} (O3) uncoordinated and thereby tilting occurs, creating a buckled

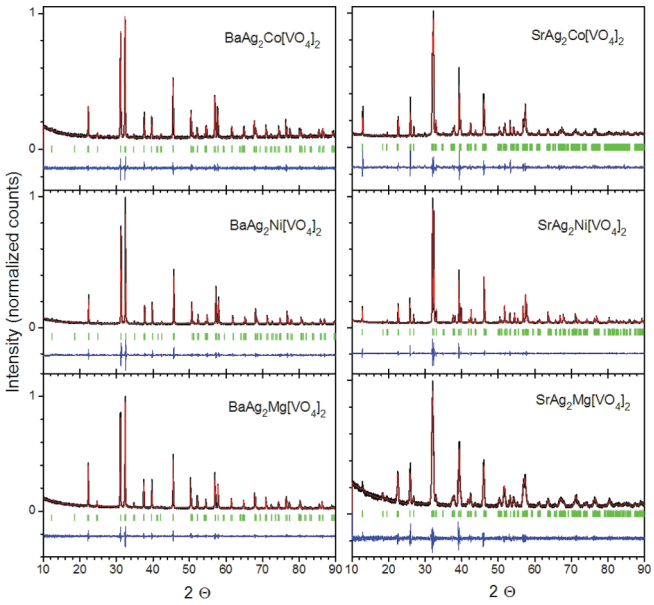

FIG. 3. (Color online) Powder diffraction data of $BaAg_2M[VO_4]_2$ (left) and $SrAg_2M[VO_4]_2$ (right) for M = Co, Ni, and Mg. Rietveld refinement (Profile matching method) with experimental (black), calculated (red), and difference (blue) intensities. The green marks reference the Bragg positions (see text for details).

oxygen atom layer in the ab plane. It is noteworthy that the triangular lattice formed by the M^{2+} ions remains planar, but the local symmetry of the transition metal coordination sphere, $[MO_6^{ab}]$, is thus reduced from D_{3d} (I) to C_i (II). These slight distortions, overall Δd(M–O^{ab}) ≈ 0.10 Å and $\Delta\angle(O^{ab}$–M–$O^{ab})$ < 5°, induce an anisotropy to the triangular lattice that should influence the respective magnetic exchange within the layers.

Since the relative orientation of the $[MO_6]$ and $[VO_4]$ units can be regarded as the main key unit for the superexchange present, we give the dihedral angles for each principal direction in the ab plane, see Fig. 2. Recently, we used a similar procedure to relate a microscopic model deduced for the magnetic exchange to structural details for $BaAg_2Cu[VO_4]_2$.[21] Since the superexchange pathway involves the vanadate, empty V d orbitals are essentially contributing. In more detail, we have found that the relative orientation of $[MO_6]$ and $[VO_4]$ units will significantly alter the effective exchange couplings, e.g., for $\varphi \approx 130°$ ferromagnetic and for $\varphi \approx 100°$ antiferromagnetic exchange results.[21] Despite the fact that the previous results were obtained for a one-electron system, we might consider this phenomenological description for the Co and Ni compounds as well. The dihedral angles φ link three M cations via a vanadate (motive of the triangular lattice) and additionally represent the respective crystallographic in-plane directions. In detail, we note that for (II) φ_2 is significantly smaller than φ_1, φ_3, and φ for (I) and might be taken as an indicator of increasingly effective AFM correlations from the M-O-O-M pathway, which eventually can match or even exceed the FM from the V d-orbital contribution. Effectively, this will render J_2 (reference to φ_2) low. All other φ indicate that ferromagnetic couplings should be dominant. For experimental results corroborating this picture see Secs. V and VI.

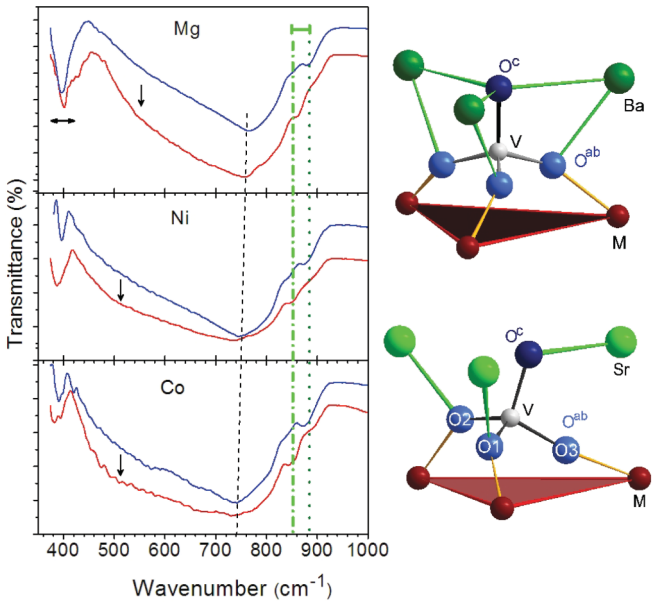

FIG. 4. (Color online) Infrared spectra for $A\mathrm{Ag}_2M[\mathrm{VO}_4]_2$ with M = Mg, Ni, Co (left) and the structural features of the coordination around the vanadate (right). Spectra related to the structure types (I) and (II) are shown in blue (A = Ba) and red (A = Sr), respectively. Guideline to the eye: the dashed (black) line represents the peak maxima related to ν_3, the vertical arrows indicate the additional shoulder of the broad feature for (II) and the dashed/dotted lines (green) mark the shift of the ν_1 related mode. The range of the bending modes is indicated by horizontal arrows (black).

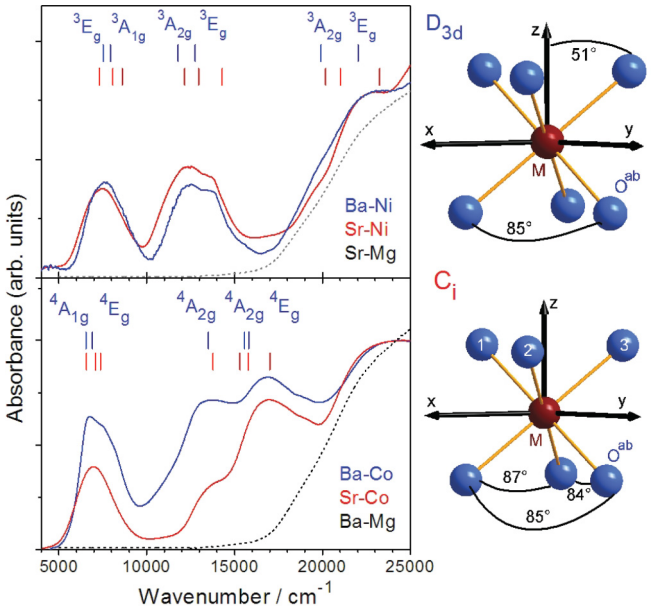

FIG. 5. (Color online) Absorbance spectra for $A\mathrm{Ag}_2M[\mathrm{VO}_4]_2$ with M = Mg, Ni, Co (left), orientation of a single ion complex, $[M\mathrm{O}_6^{\mathrm{ab}}]$, with respect to the local axes (right). Spectra related to the structure types (I) and (II) are shown in blue (A = Ba) and red (A = Sr), respectively. The Mg compounds are given for reference (dashed black lines). Guideline to the eye: bars indicate peak positions related to D_{3d} (I) and C_i (II) symmetries of the single ion complexes as calculated for spin-allowed transitions excluding spin-orbit coupling.

IV. SPECTROSCOPY

In order to study the induced structural distortion enforced on the vanadates, we used infrared (IR) spectroscopy as a local probe. For a tetrahedral species, two fundamental stretching modes ν_1 (Raman-active, nondegenerate, symmetric) and ν_3 (IR-active, triply degenerate, asymmetric) are expected. For lower symmetries such as C_{3v} (I) and C_1 (II), ν_1 becomes IR-active and ν_3 splits into two and three modes, respectively.[36] Figure 4 shows these stretching vibrations (broad feature centered at ≈750 cm^{-1}) as well as the bending modes (ν_2 and ν_4) around 380–400 cm^{-1}. Furthermore, the coordination spheres of the vanadates in (I) and (II) are depicted. It can be seen that ν_1 in the range of 845–880 cm^{-1} is related to the change in the connectivity by A atoms and the difference in interatomic distance $\Delta(V - \mathrm{O}^{\mathrm{c}})$ of ≈0.03 Å. A redshift of ν_1 of ≈25 cm^{-1} with decreasing A–O^{c} distance and more important decreasing coordination number is observed. On the other hand ν_3, featuring the O^{ab} connecting to the triangular lattice formed by M (mean distance V–O^{ab} of 1.71 Å), is not significantly altered by the A site. Hence, this mode is related mainly to the ionic radii of M^{2+} and shifts with increasing ionic size to lower wave numbers. Consequently, for each M system the main peak of ν_3 ≈740–760 cm^{-1} remains unaffected in energy regardless of A, but develops the expected additional shoulder at lower wave numbers for (II). It is interesting to note that for M = Co this shoulder in the broad peak assigned to the asymmetric stretching vibration of the vanadate is seen for (I) and (II). We believe that this reflects a somewhat lower local symmetry for the vanadate induced by the local distortion of the $[\mathrm{CoO}_6]$ complex as anticipated according to the Jahn-Teller theorem[37] in this special case, see also below. The bending modes of the vanadate in general exhibit splitting and broadening for (II) when compared with (I). Again in the M = Co case a splitting of ≈10 cm^{-1} already occurs for (I).

The evaluation of the UV-Vis spectra of the insulating nonmagnetic $A\mathrm{Ag}_2\mathrm{Mg}[\mathrm{VO}_4]_2$ compounds provide us with an estimate of the band gap of ≈2.4 eV (I) and 2.5 eV (II), respectively, using the procedure given in Ref. 38. Absorbance occurs in the blue and therefore the Mg compounds are yellow. The absorbance spectra of $A\mathrm{Ag}_2M[\mathrm{VO}_4]_2$ with M = Co and Ni are given in Fig. 5 in comparison with the Mg compounds. The additional bands in the near-infrared (NIR) and visible (vis) region originate from d-d transitions of the single ion complexes, $[M\mathrm{O}_6^{\mathrm{ab}}]$, and are evaluated within the framework of the angular-overlap model (AOM)[39–41] with parameters given in Ref. 42. The Ni compounds are yellow-brown whereas both Co compounds are dark-olive. Since the d-d bands are usually very broad, the rather small distortion from D_{3d} (I) to C_i (II) is not well resolved for the excitation bands. Angles given in Fig. 5 show the distortion from an ideal octahedron. For a trigonal crystal field, the angle with the principal z axis is used to determine the deviation from O_h symmetry (54.74°) and amounts to 51° for (I) and only slightly deviates for (II). Calculations within the AOM were carried out with the same set of bonding parameters, e_σ and e_π relating to the σ bonding and π antibonding between the metal cation and oxygen for (I) and (II), respectively, and are adjusted according to Dunn's law[43,44] for difference in interatomic distances for (II). The Racah (B, C) and spin-orbit coupling (ζ) parameters for each

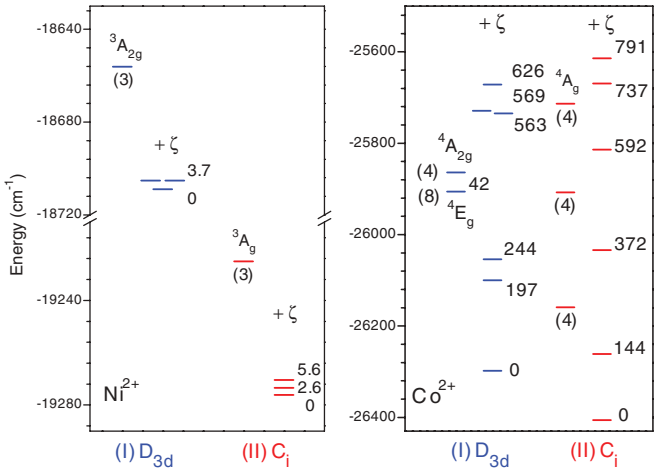

FIG. 6. (Color online) Calculated ground and low-lying excited states for the single-ion complexes, $M = Ni^{2+}$ d^8 (left) and Co^{2+} d^7 (right) in a trigonal and a slightly distorted octahedral ligand field, $[MO_6^{ab}]$, with D_{3d} (I) and C_i (II) symmetries. The numbers in brackets represent the degeneracy of the level without spin-orbit coupling. The splitting into the Kramers doublets arising from spin-orbit coupling (ζ) is shown and the relative energies with respect to the ground level set to zero are given.

metal cation were reduced by an isotropic orbital-reduction factor (k_r) to account for some covalency. This simplification allows us to reduce the number of refinable parameters and hence, facilitate a comparison between the structure types (I) and (II) once we focus on the ground state properties and the magnetic structure, see below. From the AOM calculations the energies of the excited states can be deduced for the single ion complexes and are given for D_{3d} symmetries with the spectroscopic labels in Fig. 5. The lower symmetry of C_i affords splitting of all E_g states leading to A_g spectroscopic terms. Overall, experimental data and our calculations are in good agreement and typical values of the respective octahedral ligand field splitting of $\Delta_o \approx 7500$ cm^{-1} for Ni^{2+} and 7000 cm^{-1} for Co^{2+} can be deduced for these type of compounds. Note that Δ_o is related to the bonding parameters of an undistorted octahedron and equals $\approx 4e_\sigma - 3e_\pi$.[42]

More important here are the ground-state properties, which can be deduced from our calculations, given the consistent and excellent agreement of observed transition energies within our parameter restricted simulations. Both free metal ions have F terms lowest in energy. These split in an octahedral ligand field into A_{2g}, T_{1g}, and T_{2g} terms with different spin multiplicities.[39,45] The main difference arises for ideal O_h symmetry placing $^4T_{1g}$ lowest in energy for Co^{2+} and $^3A_{2g}$ for Ni^{2+}. The single ion complexes, $[MO_6]$, exhibit ground states for $M^{2+} = Ni$ $^3A_{2g}$ (I) and ^3A_g (II), respectively, whereas in the case $M^{2+} = Co$ (I) ^4E_g and $^4A_{2g}$ with a separation of only 42 cm^{-1} result from the splitting of the $^4T_{1g}$ in an axial distorted (trigonal) ligand field, see Fig. 6. Furthermore, the ^4E_g ground state is subject to an electronic effect according to the Jahn-Teller theorem.[37,46] Thereby, the degeneracy is being lifted and an additional (local) distortion of the single-ion complex will occur. This might be small and overlooked in a x-ray experiment, which is based on translation symmetry. The distortion present in (II) on the other hand would lift the orbital degeneracy of the ^4E_g ground-state directly.

Figure 6 shows the result of our ligand-field calculations on the ground state including spin-orbit splitting, as well as first- and second-order Zeeman effects up to 12 000 cm^{-1}. It can be seen for Ni^{2+} that the ground state is split by spin-orbit coupling into three Kramers doublets overall separated by 3.7 (I) and 5.6 cm^{-1} (II). With the important result that the two excited levels are thermally accessible and will introduce some anisotropy only at low temperatures causing a deviation from the Curie law, see below. Consequently, one should notice subtle differences in the susceptibility in comparing (I) and (II). The situation for the Co compounds is more complicated. For the ground state ^4E_g in D_{3d} symmetry, the orbital momentum is not entirely quenched. From the two levels of ^4E_g and one of $^4A_{2g}$, six Kramers doublets (in total twelve states) arise when spin-orbit coupling is applied in an energy range of $\approx$800 cm^{-1}, which is overall beyond the limit for thermal occupancy in our experimental range up to 300 K. Even the energy difference between the two lowest Kramers doublets suggests that thermal occupancy is established only at high temperatures (T around 150 K), see Fig. 6. Consequently, the temperature dependence of the reciprocal susceptibility does not follow a simple Curie law of a spin-3/2 system. Hence, peculiar anisotropic magnetic behavior occurs in the entire temperature range studied and justifies a formal description of a $S^{\text{eff}} = 1/2$ spin system for Co^{2+}, see below.

Our calculations of the ground-state properties including spin-orbit splitting and the angular dependence of the ligand field let us derive the anisotropy of the temperature-dependent susceptibility for a single-ion complex with no magnetic couplings considered (paramagnetic case), see Sec. V. Two different situations arise with the main magnetic moment for Ni in the ab plane and perpendicular to the triangular layer for Co, see Sec. VIII confirming this evaluation.

V. MAGNETIC PROPERTIES

First, we will discuss the Ni compounds. For both structure types (I) and (II), we find the expected Curie-type behavior of $1/\chi$ proportional T of a spin-1 system at high temperatures (see Fig. 7) with a g value of 2.12 originating from the first-order Zeeman effect with $g = 2.00(1 + 2\zeta/\Delta_o)$, where ζ and Δ_o represent the spin-orbit coupling constant and the octahedral ligand field splitting, respectively. See also Fig. 8 for the value of the saturation magnetization, M_S, indicating $g \approx 2.12$. For the experimental reciprocal susceptibility, $1/\chi$, deviation from the Curie law occurs below 120 K and can be attributed to short-range order, here, ferromagnetic coupling within the triangular layers. Effective Curie-Weiss temperatures, $\Theta_{\text{C.W.}}$, around 10 K (I) and 6 K (II) can be derived. Since $\Theta_{\text{C.W.}}$ is a linear combination of different exchange couplings, this shift in temperature for (II) can be considered direct evidence for the overall reduction of the effective exchange couplings present and corroborates the influence of the exchange pathway linked to φ_2 becoming less FM or even AFM.

A closer inspection (inset bottom right of Fig. 7) gives the susceptibility measured at a field of 100 Oe below 20 K and reveals the difference in T_c of 4 K between (I) and(II) with $T_c \approx 10$ and 6 K, respectively. Note that $\Theta_{\text{C.W.}}$ and T_c are

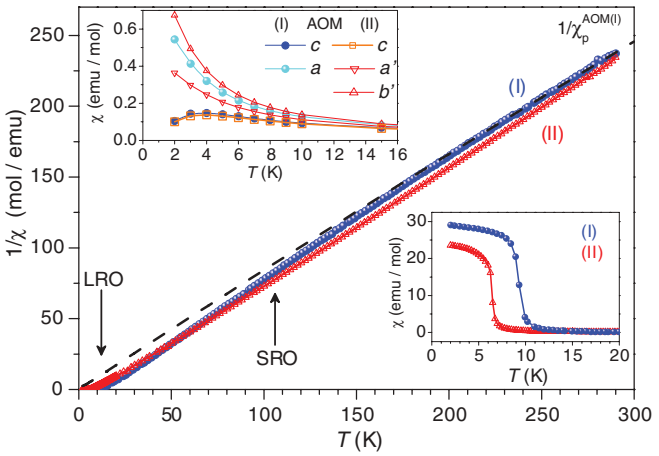

FIG. 7. (Color online) The main panel shows the experimental reciprocal susceptibility measured at 100 Oe for (I) $BaAg_2Ni[VO_4]_2$ (blue bullets) and (II) $SrAg_2Ni[VO_4]_2$ (red triangles) in comparison with the calculated powder data (denoted $1/\chi_p^{\mathrm{AOM(I)}}$, black dashed line). The inset (left top) includes the calculated (AOM) single-ion anisotropic behavior of χ(T) with references to the crystallographic axis for the two structure types [(I), blue and cyan) and (II), red]. The inset (right bottom) depicts the susceptibility (100 Oe) in the low-temperature range for (I) $BaAg_2Ni[VO_4]_2$ (blue bullets) and (II) $SrAg_2Co[VO_4]_2$ (red triangles) with $\Delta T_c \approx 4$ K.

approximately equal, suggesting absence of or reduced frustration. However, long-range order (LRO) and the single-ion anisotropy, resulting from zero-field splitting or as referenced in Fig. 6 by spin-orbit coupling, are effective in the same temperature region. The top inset of Fig. 7 shows the calculated anisotropy of χ(T) below 16 K. It can be seen that $\chi_c(\mathrm{T})^{\mathrm{AOM}}$ is not altered by the structural distortion, whereas the main magnetic moment lying in the ab plane exhibits a significant different behavior. Note that we choose to reference the molecular x and y direction of a single-ion complex as a and b for simplicity here. For (II), the anisotropy in the ab plane is evident and

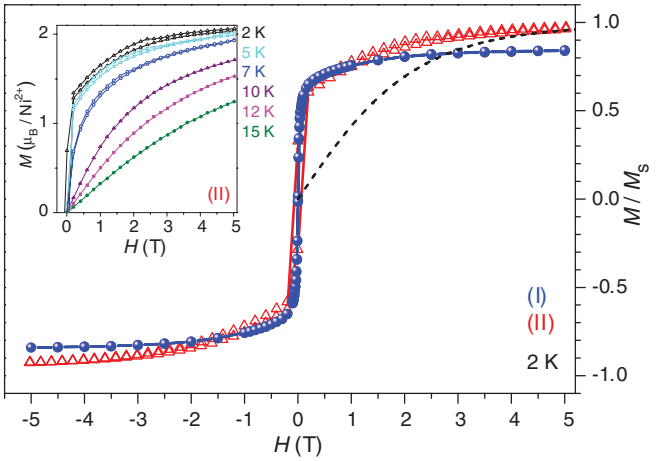

FIG. 8. (Color online) The main panel shows the field dependent magnetization data, M/M_s for (I) $BaAg_2Ni[VO_4]_2$ (blue bullets) and (II) $SrAg_2Ni[VO_4]_2$ (red triangles) at 2 K with the Brillouin function (black dashed line) shown for comparison. The inset depicts M(H) of (II) at 2, 5, 7, 10, 12, and 15 K, respectively.

recalling the dihedral angles discussed above will certainly alter the magnetic properties, see temperature difference in T_c.

On passing we should add, that any change to the magnetic exchange along c is not mediated by the temperature behavior of the (molecular) $\chi_c(\mathrm{T})^{\mathrm{AOM}}$, but rather a result of the different stacking orientations of the magnetic layers along the c axis. For (II), this stacking is alternating with respect to the relative (molecular) z orientation (see Figs. 1 and 5) by a small angle off the crystallographic c axis. This opposite tilting (canting) of adjacent layers may be considered as a contribution to lower T_c effectively for (II). Overall, couplings along c can be assumed to be fairly weak. This is supported by the discussed anisotropy at low temperatures and by neutron diffraction data (see Sec. VIII).

Field-dependent magnetization data is shown in Fig. 8 at 2 K for $BaAg_2Ni[VO_4]_2$ (I) and $SrAg_2Ni[VO_4]_2$ (II). A comparison with the Brillouin function for a spin-1 system (g value is 2.12) indicates dominant ferromagnetism present, with small coercive fields of ≈10 Oe. Initial very low fields lead to a value of $M/M_S \approx 0.7$ for both structure types and upon further increasing fields saturation around 2 T is reached. We will comment on the lower M/M_S value for (I) in Secs. VII and VIII below. The field dependence of the magnetization of (II) is shown for several temperatures in the inset and indicates the magnetic phase transition (LRO) occurring between 5 and 7 K, see also specific heat measurements Sec. VI.

On the contrary, a more complex situation arises for the Co compounds if we consider the ground state splitting by spin-orbit coupling, see Sec. IV. Consequently, the temperature dependence of the reciprocal susceptibility does not follow a simple Curie law, see inset Fig. 9, and suggests the ground state with $|\pm\frac{1}{2}\rangle$ far below the first excited state. The calculated

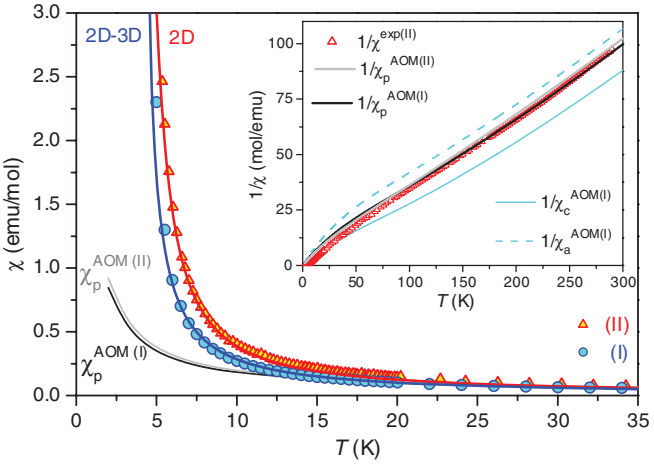

FIG. 9. (Color online) Experimental susceptibilities [blue circles (I) and red triangles (II)] measured in a field of 100 Oe in comparison with calculated (paramagnetic) χ_p^{AOM} data for (I, black) and (II, grey) in the low-temperature range. The solid lines represent data for a $S^{\mathrm{eff}} = 1/2$ Ising system with dominant ferromagnetic 2D couplings $J^{\mathrm{ab}} = -4.0$ K (II, red) and a 2D-3D model with $J^{\mathrm{ab}} = -2.5$ K including $J^{\mathrm{c}} = -0.1$ K (I, blue). (Inset) Experimental data for $SrAg_2Co[VO_4]_2$ (red triangles) in comparison with the calculated temperature dependence of the reciprocal susceptibilities: average $(1/\chi_p^{\mathrm{AOM}})$ for (I, black) and (II, grey), and $1/\chi_a^{\mathrm{AOM}}$, $1/\chi_c^{\mathrm{AOM}}$ (dashed and solid cyan lines) for D_{3d}.

(molecular) anisotropic behavior of $1/\chi^{\mathrm{AOM}}$(T) in the ab plane and along the c axis are depicted for (I) and clearly show that the temperature dependence around 50 K is not a signature of magnetic correlations. Furthermore, it can be seen that the main magnetic moment is along the c axis (molecular z direction), well in line with an effective spin-1/2 system below ≈25 K. If we now compare the calculated average powder data, $1/\chi_p^{\mathrm{AOM}}$(T), for (I) and (II) no subtle difference is noticeable down to the lowest temperature and our experimental data, in principal, follow the single ion behavior above 20 K. The small difference arises from the calculated g_{av} values of 4.2 (I) and 4.4 (II), respectively, with molecular g values of $g_{\parallel} = 5.14$ (I) or 6.54 (II) and $g_{\perp} = 3.66$ (I) or 2.10, 3.17 (II).

As previously mentioned for the Ni compound, we find a slight deviation from the single-ion behavior below 100 K for the Co compounds as well, indicating ferromagnetic short-range correlations leading to intercepts on the temperature scale at around 4.2 K ($\Theta_{\mathrm{C.W.}}$). Again $\Theta_{\mathrm{C.W.}}$ and T_c are found to be almost equal. Furthermore, the temperature dependence of $1/\chi$(T) is surprisingly similar for both structure types (I) and (II) and given here for the measurements taken at a field of 100 Oe. Note that the very low temperature range for χ(T) is shown in comparison with our neutron diffraction results in Fig. 16 of Sec. VIII.

The main panel of Fig. 9 reveals the deviation from the (paramagnetic) single-ion susceptibility [χ_p^{AOM}(T)] at temperatures below 20 K and reflects the magnetic exchange interactions. Recalling that the main magnetic moments of the single-ion complex for $M = \mathrm{Co}^{2+}$ are oriented parallel to the c axis, a $S^{\mathrm{eff}} = 1/2$ spin system is present, and the molecular g values are very different, we suggest that a description within the Ising model is justified. Hence, it is expected that the in-plane exchange constant J_{ab} is related to T_c by a factor of 1.0986.[47] With $T_c = 4.2$ K, as derived also from the maximum in C_m/T in zero field (see Sec. VI) and from neutron diffraction for (I), we estimate $J_{\mathrm{ab}} \approx -4.5$ K for the Co compounds. Figure 9 shows the result of the calculated temperature dependence of the susceptibility for a 2D Ising model using a high-temperature series expansion[48,49] with $g = 4.2$ and $J_{\mathrm{ab}}^{(\mathrm{II})} = -4.0$ K in excellent agreement with the experimental data. For (I), we note that the onset of the divergence of the susceptibility is shifted to lower temperatures, suggesting a smaller effective value for $J_{\mathrm{ab}}^{(\mathrm{I})}$ of ≈−2.5 K for the 2D model, well in line with the above φ value of 118° (I) compared to the larger ones of 130° and 147° (II) along the a and b direction, respectively. Based on the following observations for $BaAg_2Co[VO_4]_2$: (i) the steeper divergence of $\chi^{(\mathrm{I})}$ and (ii) lower values for the field-dependent magnetization (see Fig. 10) if compared with $SrAg_2Co[VO_4]_2$, we propose a quasi-2D Ising model with small but sizable interlayer couplings (3D) for (I). Using Eq. (3) from Ref. 50 for a 2D-3D Ising model, a reasonable fit to the data can be obtained by introducing $J^{\mathrm{c}} \approx -0.1$ K as the upper limit.

Figure 10 shows the experimental field dependent magnetization for $BaAg_2Co[VO_4]_2$ and $SrAg_2Co[VO_4]_2$. At all temperatures the latter one reveals slightly larger M(H) values. This is in line with the larger (i) g value as obtained from the AOM and (ii) ferromagnetic J^{ab} intraplane coupling. Furthermore, we note that below T_c and 2 T the difference

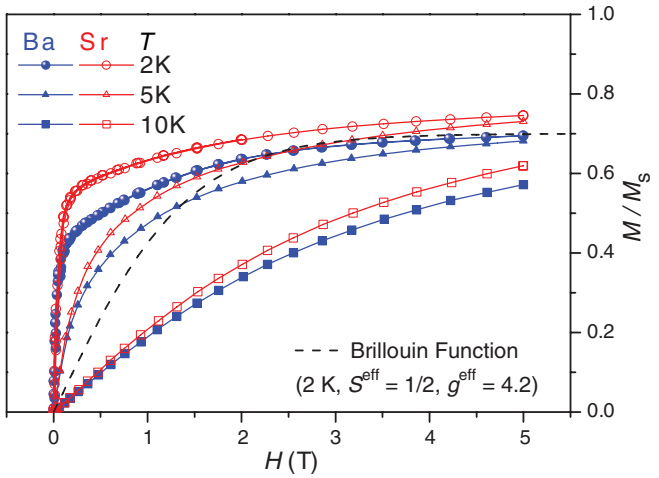

FIG. 10. (Color online) For (I) $BaAg_2Co[VO_4]_2$ (blue) and (II) $SrAg_2Co[VO_4]_2$ (red) the field-dependent magnetization divided by the saturated magnetization for a spin-3/2 system, M/M_s, is given at temperatures of 2, 5, and 10 K, respectively. For comparison, the Brillouin function (black dashed line) for an effective spin-1/2 system is plotted for 2 K.

in M(H) is more pronounced, which is reflective of the respective J^{ab} and J^{c} couplings. On the other hand both compounds display rather similar behavior at 2 K (above 2 T), 5, and 10 K, supporting our model of a 2D Ising system with differences in the rather small 3D exchange couplings. Similar to the Ni compounds the magnetization approaches a plateau around 2 T and a small coercive field, e.g., 19 Oe in the case of $BaAg_2Co[VO_4]_2$, has been derived. For reference, we show the Brillouin function for an effective spin-1/2 system at 2 K, which is considered for the Ising model here. Above 2 T, the magnetization continuously increases, since the saturation for a $S = 3/2$ is not yet reached.[51] This observation is not unexpected, because the splitting between the two lowest Kramers levels is large, see Fig. 6, and therefore, rather a measure of the spin-orbit splitting than an indicator for additional magnetic correlations. Similar findings of low magnetic moments at low fields (around 5 T) are typical for an effective spin-1/2 system and have been reported for other layered Co compounds, see, for example, Ref. 50.

Despite the observation that the Co compounds exhibit rather similar features in all studied experiments, the underlying phenomenological description is slightly different. Whereas for (II) a nearly ideal 2D Ising behavior on the triangular lattice is indicated here, minor correlations between the layers are in effect for (I). Since the structure of (I) is shown to have a stacking of identical layers, structure type (II) not only exhibits a distortion, but also a tilting off the c axis, thus resulting in two different orientations of adjacent triangular lattices and thereby an alternating stacking order occurs. This may be regarded as the main key to understand why the interplane coupling for (II) renders low or even vanishes to resemble a quasi 2D Ising behavior on the triangular lattice.

VI. SPECIFIC HEAT

The evaluation of our specific heat measurements at different fields are illustrated in Fig. 11 for the Co and

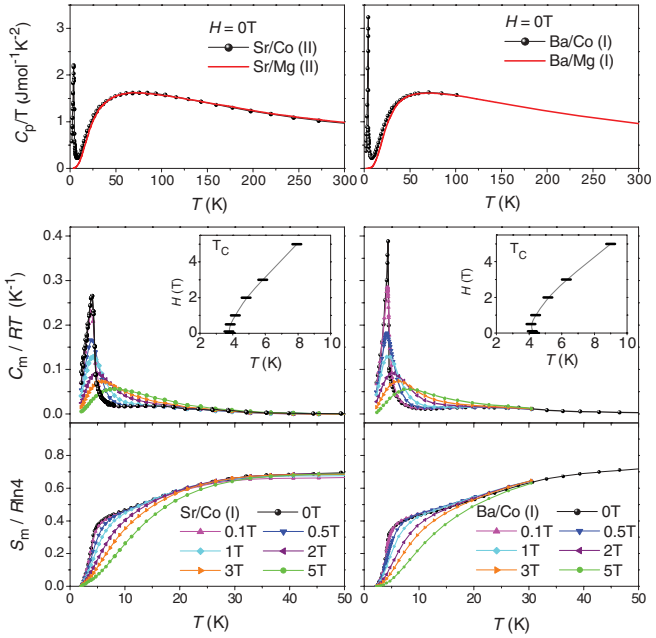

FIG. 11. (Color online) The top panels show the experimental zero-field specific heat divided by the temperature (black bullets) of (II) $SrAg_2Co[VO_4]_2$ (left) and (I) $BaAg_2Co[VO_4]_2$ (right). The modified data for the respective Mg compound (red lines) has been used to determine the lattice contribution to the specific heat, see text. The middle panels show the derived magnetic contribution at different fields to the specific heat C_m divided by the temperature and the gas constant R. The insets give the field dependence of the anomaly T_c. The bottom panels show the scaled magnetic entropy for different fields.

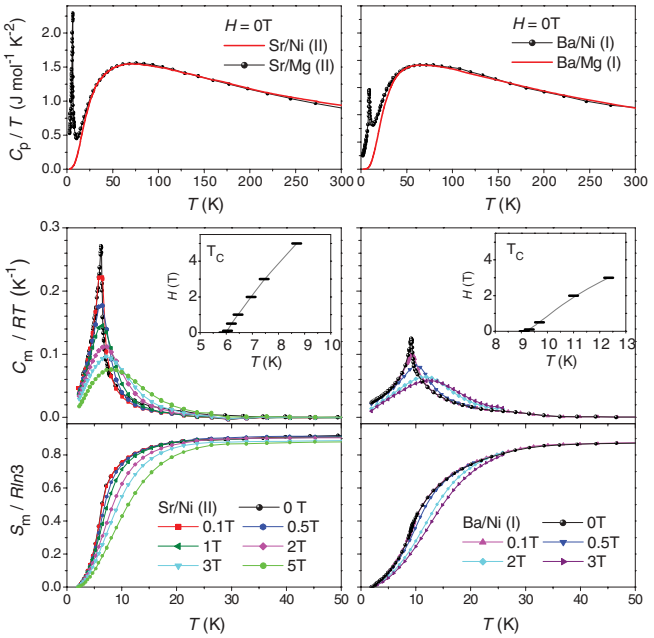

FIG. 12. (Color online) The top panels show the experimental zero-field specific heat divided by the temperature (black bullets) of (II) $SrAg_2Ni[VO_4]_2$ (left) and (I) $BaAg_2Ni[VO_4]_2$ (right). The modified data for the respective Mg-compound (red lines) has been used to determine the lattice contribution to the specific heat, see text. The middle panels show the derived magnetic contribution at different fields to the specific heat C_m divided by the temperature and the gas constant R. The insets give the field dependence of the anomaly T_c. The bottom panels show the scaled magnetic entropy for different fields.

in Fig. 12, for the Ni compounds. The total specific heat divided by the temperature, C_p/T, is given in the top panels, respectively. To account for the lattice contributions to the total specific heat, we use the modified respective Mg compounds (nonmagnetic) to extract the magnetic part of the specific heat, (C_m^M with $M =$ Co, Ni), for details see Ref. 52. The magnetic entropy S_m of each system is derived by integrating the respective C_m^M/T data.

First, we will discuss our results for the Co compounds. We have described the magnetic properties within the model of a 2D Ising spin-1/2 system in the previous section. According to the underlying theory,[53] conventional long-range order exists in these systems. Figure 11 indeed shows a sharp anomaly, which can be assigned to a LRO transition with T_c at approximately 4.2 K in zero field. The field dependence of $C_m/(RT)$ versus the temperature featured in the middle panel exhibits a shift to higher temperatures as well as the onset of significant broadening once the field is increased, indicative of leading ferromagnetic correlations being present. The different shape of the anomalies at zero-field seem to indicate a more pronounced 2D character for (II). The insets show the field dependence of T_c and as noticed above a rather similar behavior is evident for (I) and (II).

The magnetic entropy divided by $R\ln(2S+1)$ ($=R\ln 4$) for the Co compounds is depicted in the bottom panel of Fig. 11. In zero field, the typical kink around T_c is observed and $S_m/R\ln 4$ approaches a plateau with a value of 0.4 ($S_m \approx$ 5.0 J mol^{-1}K^{-1}), representing about 85% of the expected one for a $S^{\text{eff}} = 1/2$ system, which is in line within the Ising model considered here. Note that the temperature range below 2 K is not measured, therefore some contribution to S_m remains unconsidered and effectively renders the total values somewhat lower. Around 30 K, all entropy curves follow a single line and increase up to 70% of the total entropy for a spin-3/2 system, well in line with the previous discussion.

Now, we comment on the increase in S_m between 10 and 30 K of ≈20%. Since almost the entire magnetic entropy of a FM $S^{\text{eff}} = 1/2$ system is released in the temperature region below approximately 10 K, we need to consider a different origin for the higher temperature regime. The temperature-dependent behavior C_m/R of $BaAg_2Co[VO_4]_2$ is shown in the inset of Fig. 13 and the Onsager solution for $T \leqslant T_c$ is given for reference to a spin-1/2 triangular lattice. Additionally, a broad feature around 22 K is clearly noticeable for the Co-compound (I), as shown in the inset of Fig. 13, and has been observed for (II) as well. Thus we propose the assignment to a so-called Schottky anomaly, arising from the splitting of the two lowest Kramers levels with a separation in energy of approximately $k_r^2 \times 150\,\text{cm}^{-1} = 95\,\text{cm}^{-1}$ in agreement with our estimate of 85 cm^{-1} from $T_{\text{max}}^{\text{Schottky}}$. See also the temperature dependence of the reciprocal susceptibility (see Fig. 11) for the slope change around 25 K. We tend to favor this scenario, however, it cannot be ruled out that SRO might be considered as one alternative origin altogether.

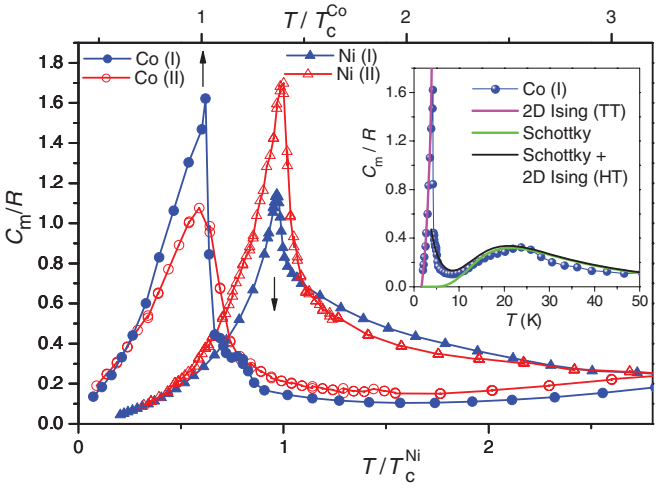

FIG. 13. (Color online) The main panel shows the experimental magnetic specific heat divided by the gas constant R in zero field for $BaAg_2M[VO_4]_2$ (I) and $SrAg_2M[VO_4]_2$ (II) vs the normalized temperature T/T_c. The inset gives the comparison of the experimental data for $BaAg_2Co[VO_4]_2$ (blue circles) with the low-temperature solution for a 2D Ising model (magenta), the high-temperature feature related to a Schottky anomaly (green) as well as the sum of the high-temperature 2D Ising model and the Schottky anomaly (black).

The experimental total specific heat, magnetic part of the specific heat and entropy for $AAg_2Ni[VO_4]_2$ are depicted in Fig. 12. It can be seen that S_m(T) approaches the expected value for a spin-1 system above 30 K. Furthermore, the shape, the absolute temperature of the anomaly, see C_m(T), and as shown in the inset the field dependence of maxima in zero and applied fields differ significantly for (I) and (II). Overall, the specific heat for the Ni compounds is very different from the Co compounds (see Fig. 13), which can be readily understood on the basis of their respective ground state properties. Whereas, the latter has been described within the theory of an Ising model, a Heisenberg model seems to be more appropriate for the Ni compounds, given the almost isotropic g values. The main in-plane magnetic moment for the Ni compounds suggest the consideration of a XY model as a possible alternative to account for the anisotropic case (II), see structural distortions (see Table I). However, for both Heisenberg models conventional LRO at finite temperatures is not predicted by theory.[54–56]

Two leading contributions may be considered to reintroduce LRO, e.g., interplane correlations along c (J^c) and splitting of the ground state by spin-orbit coupling or zero-field splitting. Both may play a significant role and need to be considered below 15 K. As previously discussed for the Co compounds, the layer stacking in a unique fashion (I) evokes some small interlayer coupling, whereas for (II) the tilted alternating stacking pattern renders this exchange effectively lower. Thus, in accordance with the, by orders of magnitude lower, J_c compared with J_{ab}, no significant shift for T_c is noticeable for the Co samples. This leaves the single ion in-plane anisotropy of the spin-1 system to be the most likely origin of the drastic reduction of T_c by almost 4 K in $SrAg_2Ni[VO_4]_2$ in comparison with $BaAg_2Ni[VO_4]_2$. However, the calculated splitting of the ground state yields the $|0\rangle$ level lowest in energy for the Ni compounds, with the energy difference to the other two components ($|\pm1\rangle$) smaller or almost equal to $|J_{ab}|$. Hence, one may expect a divergence of the intraplane correlation length at nonzero temperatures, which could give rise to a singularity in the specific heat.

Let us now discuss the difference in T_c's for the Ni compounds or even more useful here in terms of $\Theta_{C.W.}$ of $\approx$6 K (II) and 10 K (I), respectively. Recalling that $\Theta_{C.W.}$ is representing the sum of all J couplings and relating this to structural aspects by the above given angles, denoted φ, we may conjure a rather unexpected outcome for the spin-1 Heisenberg model on the triangular lattice here. Isotropic FM couplings are expected for (I), in contrast to (II) where a closer inspection yields FM $J_a \simeq J_b$ with the diagonal component J_{ab} possibly AFM. This would then represent a frustration to the triangular lattice with next-nearest bonds FM (4×) and AFM (2×) in the extreme limit, suggesting a reduction of $\Theta_{C.W.}$ by about 1/3. Note that $|J^{FM}|$ is anticipated to be larger than $|J^{AFM}|$ as well as $|J_{FM}^{(II)}| > |J_{FM}^{(I)}|$. Clearly, the Heisenberg model will be very susceptible to such a pattern with the proposed couplings. In a phenomenological picture this would explain the lower $\Theta_{C.W.}$ for (II) and in fact the ratio $\Theta_{C.W.}^{(II)}/\Theta_{C.W.}^{(I)}$ is found to be close to 2/3.

VII. PRESSURE DEPENDENCE OF T_c

In order to get more insights into the underlying phenomena discussed above and to investigate any possible role of the alkaline earth ionic size, as described in Sec. II, we carried out pressure-dependent ac magnetic susceptibility (χ_{ac}) measurements and determined the change of the FM transition temperatures with pressure. The ac susceptibility at ambient pressure, as shown in Fig. 14 for all compounds, reveals a sharp increase and a peak at the FM transition. Upon increasing pressure, the peak of χ_{ac} shifts to higher temperatures, but at different rates. The relative shifts of T_c with pressure are displayed in Fig. 15. The increase is significant for all compounds, up to 12% at 1.9 GPa in $BaAg_2Ni[VO_4]_2$. However, there exist subtle differences between the two structures (I) and (II) as well as the magnetic ions Co^{2+} and Ni^{2+}.

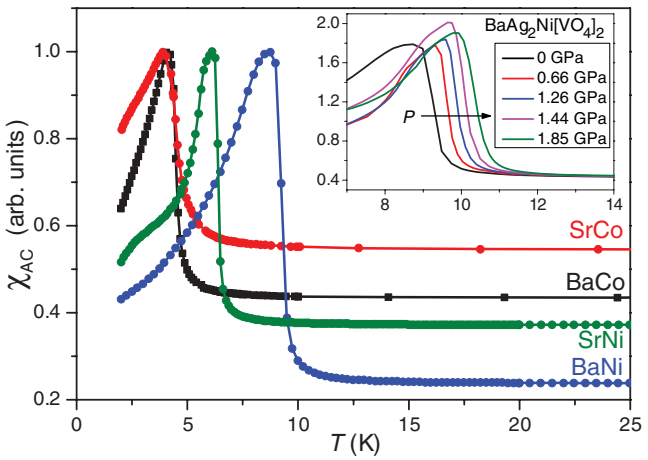

FIG. 14. (Color online) Alternating current magnetic susceptibilities χ_{ac} of the title compounds at ambient pressure. (Inset) Pressure dependence of χ_{ac} of $BaAg_2Ni[VO_4]_2$.

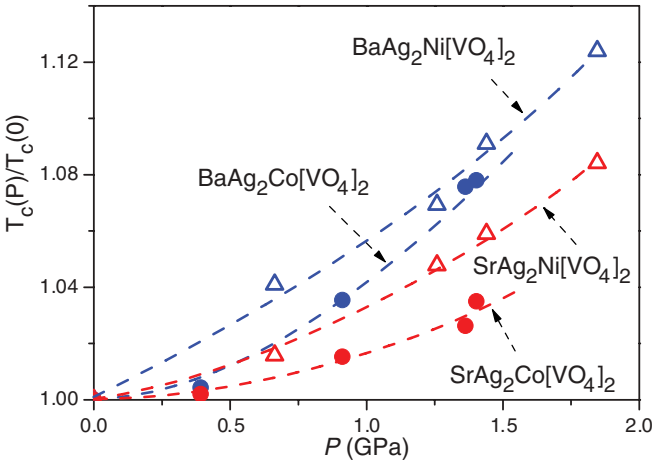

FIG. 15. (Color online) Pressure dependence of the FM transition temperatures T_c of the title compounds. The dashed lines are only a guide to the eye.

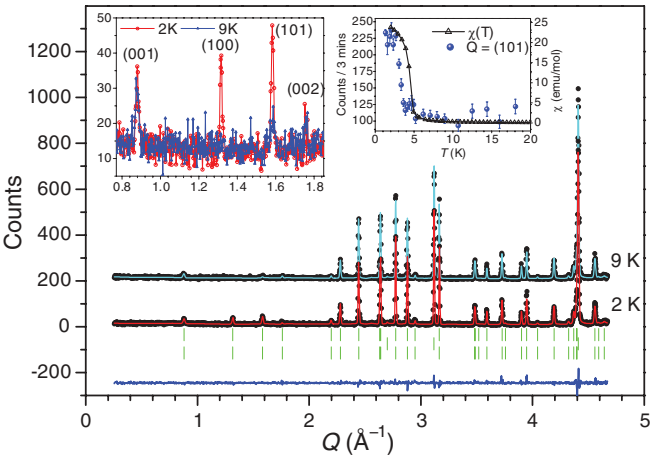

FIG. 16. (Color online) Neutron powder diffraction data for $BaAg_2Co[VO_4]_2$ at 2 and 9 K (offset by 200 counts) with the structural (above) and magnetic (below) Bragg positions given as green lines (the middle symbols correspond to the container material, Al). The bottom line (blue) gives the difference in intensity between the experiment at 2 K and the refined model. (Left inset) Enlargement shows the intensity change above and below T_c for selected reflections. (Right inset) Temperature dependence of the order parameter of the magnetic intensity at $Q = (101)$ Bragg peak in comparison with the magnetic susceptibility $\chi(T)$.

The higher symmetric structures (I) show a stronger response to the external pressure with the largest increase of $T_c(P)/T_c(0)$ for $BaAg_2Ni[VO_4]_2$, the compound with the highest ambient pressure T_c. The raise of T_c indicates an increase of the effective FM exchange coupling constants which are controlled mainly by the dihedral angles shown in Fig. 2. However, to better understand the effects of lattice compression for all compounds (I) and (II), a more detailed discussion is needed. At ambient pressure, the substitution of Sr for Ba results in a significant reduction of the volume by approximately 3%.

One might be tempted to explain the changes of T_c for the Ni system as a chemical pressure effect, scaling T_c with the volume. This would be in contradiction with the increase of T_c for all systems upon further compression through physical pressure. Evaluating the structural data it becomes obvious that there is an important difference between physical and chemical pressures (Sr substitution); the latter is by far not isotropic, the in-plane distances expand while the c axis is compressed significantly. Physical pressure will compress both, the c axis as well as the in-plane lattice parameters. The question arises which structural parameters determine the magnitude of the critical temperatures T_c.

At ambient pressure, the highest T_c of 9.3 K is achieved for $BaAg_2Ni[VO_4]_2$, the compound with the smallest in-plane lattice parameter (5.508 Å). This compound also shows the strongest relative increase of T_c under physical pressure (see Fig. 15). Upon increasing in-plane lattice constants, T_c systematically decreases to 6.4 K ($SrAg_2Ni[VO_4]_2$), and about 4.5 K ($BaAg_2Co[VO_4]_2$ and $SrAg_2Co[VO_4]_2$). A similar tendency is also observed for the magnitude of the pressure coefficient which increases with decreasing dimension of the ab plane. This leads us to conclude that the critical temperature for the FM order is mainly determined by the in-plane lattice parameters.

It was recently shown for the related compound $BaAg_2Cu[VO_4]_2$ that the relevant magnetic exchange coupling constants depend strongly on the dihedral angles similar to those labeled in Fig. 2. Extended microscopic calculations have revealed a competition between AFM (due to virtual electron hopping) and FM (Hund's rule coupling) interactions.[20] Changing the dihedral angle mainly tunes the AFM coupling and affects the effective exchange interaction that can eventually give rise to magnetic orders at low temperature. It seems conceivable to assume that the compression of the in-plane lattice constants results in a change (possibly increase) of some dihedral angles and an enhancement of the FM correlations. This conjecture could be confirmed by detailed structural investigation under high-pressure conditions.

VIII. NEUTRON DIFFRACTION

Neutron diffraction data for $BaAg_2M[VO_4]_2$ have been collected for M^{2+} = Co and Ni. The temperature-dependent measurements (see Fig. 16) for $BaAg_2Co[VO_4]_2$ indicate that the intensity gain below T_c is on the nuclear Bragg peak positions and thus long-range FM order is present. Nuclear (00l) peaks remain unchanged at all temperatures suggesting the spins to lie along the c axis, hence, corroborating our description above. The order parameter scan of the magnetic intensity at $Q = (101)$ resembles the afore shown χ(T) behavior, see inset Fig. 16. At $T = 1.3$ K the cell parameters were refined to $a = b = 5.51353(7)$ Å and $c = 7.1423(2)$ Å with $m(Co^{2+}) = 1.34(4)\,\mu_B$ (Bragg R factor = 4.78, magnetic R factor = 7.49, conventional Rietveld R factors: $R_{wp} = 19.5$, $R_{exp} = 15.71$, and $\chi^2 = 1.54$).

Additionally, we have carried out simulations for the Co compound of a scenario that includes an AFM in-plane order and canting along the c axis that could consequently mimic the magnetic properties of a FM. However, we find no evidence from our neutron diffraction data within the experimental precision limit of an AFM moment of $\approx$0.3 μ_B. We have not observed any $hkl \pm (0.5,0.5,0)$ satellites as would be

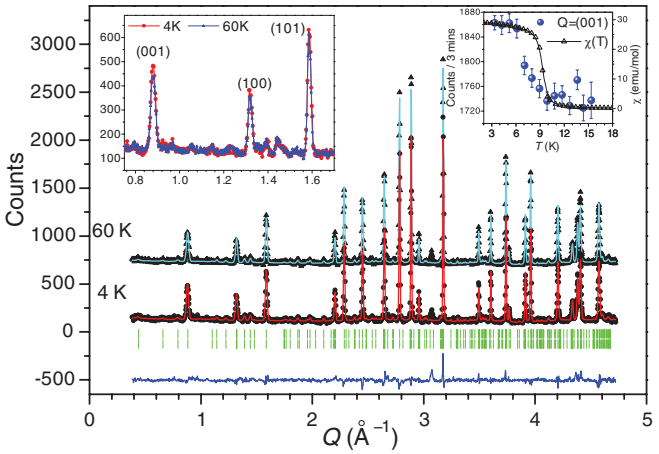

FIG. 17. (Color online) Neutron powder diffraction data for $BaAg_2Ni[VO_4]_2$ at 4 and 60 K (offset by 600 counts) with the structural (above) and magnetic (below) Bragg positions given as green lines. The bottom line (blue) gives the difference in intensity between the experiment at 4 K and the refined model. (Left inset) Enlargement shows the intensity change above and below T_c for selected reflections. (Right inset) Temperature dependence of the order parameter of the magnetic intensity at $Q = (001)$ Bragg peak in comparison with the magnetic susceptibility $\chi(T)$.

required for AFM in-plane order. Therefore, the experimental data support the above proposed FM case of the SRO and LRO.

For $BaAg_2Ni[VO_4]_2$, we find the temperature dependence as well on nuclear Bragg peak positions confirming FM-LRO, see Fig. 17. But in this case, the spins mainly lie in the ab plane. Note that the direction within the plane cannot be unambiguously determined in this symmetry because of the degeneracy. Here, we choose the diagonal direction for the refinement. The order parameter scan of the magnetic intensity is thus given at $Q = (001)$. The refinement of the magnetic phase reveals an interesting feature, which is consistent with a magnetic structure presenting a slight canting of the spins about the ab plane by approximately $+4^\circ$ to -11°. The cell parameters were refined at $T = 3.6$ K to $a = b = 5.49594(3)$ Å and $c = 7.12235(8)$ Å with $m(Ni^{2+}) = 1.16(9)\,\mu_B$ (Bragg R factor = 7.82, magnetic R factor = 8.05, conventional Rietveld R factors: $R_{wp} = 18.2$, $R_{exp} = 9.14$, and $\chi^2 = 3.95$).

Overall, the neutron diffraction data support our previous interpretations. Furthermore, the observed magnetic moments are in line with our calculations for the single-ion complexes and corroborate the consideration of an Ising model for the Co and a Heisenberg model for the Ni compound. LRO is confirmed and hence some sizable interlayer couplings are present. The observed canting for the spin-1 system, $BaAg_2Ni[VO_4]_2$, seems to be connected to the divergence from planarity on the triangular lattice. This aspect needs further consideration by other methods such as spectroscopy in order to gain more insights into the origin of the anisotropy leading to the nonplanarity here.

IX. DISCUSSION AND SUMMARY

We have investigated a series of compounds, $AAg_2M[VO_4]_2$ with $A^{2+} = Sr$ or Ba and $M^{2+} = Co$, Ni, and Mg (nonmagnetic for reference). The former magnetic members belong to the rare class of FM insulators representing a spin-3/2 and a spin-1 system, respectively. Importantly, the magnetic exchange occurs via the bridging vanadates on a triangular lattice, which apparently lead to the occurrence of FM due to the relative orientation of the transition metal centered octahedra and tetrahedra described here by the dihedral angles φ. Thus these are examples for the importance of empty vanadium d-orbitals mixing in and thereby presenting an interesting aspect of superexchange interactions. Further work will be necessary to get more insights into the presumably frustrated 2D FM order for $SrAg_2Ni[VO_4]_2$.

Based on our spectroscopic measurements and ligand field calculations, insights into the ground-state properties of the single-ion complexes are obtained. These facilitate the phenomenological description of our experimental data, $M(T,H)$ and $C_m(T)$, for the spin-systems within an Ising ($S^{eff} = 1/2$) and a Heisenberg ($S = 1$) model, respectively. Further proof of the magnetic structure is obtained from neutron diffraction data, which is well in line with the magnetic moments aligned parallel to the c axis (Co compounds) and in-plane for the Ni compounds. Note that the latter represents a degenerate set of orientations that result from the threefold rotation symmetry element that is present for the space group (I). Overall, we find pronounced 2D-FM characteristics for all magnetic members of the series with the occurrence of FM-LRO induced by the single-ion anisotropy. Furthermore, we present evidence for tuning the effectively rather small LRO by application of (i) anisotropic chemical pressure, see distortion resulting in an alternating stacking sequence of layers in structure type (II), and (ii) isotropic physical pressure. In conclusion, we have been able to provide a robust structural template, here, the geometrically frustrated triangular lattice, that allows studies into various spin-systems with exchange couplings and single-ion anisotropy on comparable energy scales.

ACKNOWLEDGMENTS

We are grateful for the generous support from the Texas Center for Superconductivity and the Welch Foundation (Grant G099857). A.M. acknowledges funding from the National Science Foundation (Grant NSF-DMR-114989). Part of this work was performed at ORNL's HFIR, sponsored by the Scientific User Facilities Division, Office of Basic Energy Sciences, US Department of Energy.

*amoeller@uh.edu

[1] E. Dagotto, Science **309**, 257 (2005).
[2] A. Ramirez, Annu. Rev. Mater. Sci. **24**, 453 (1994).
[3] G. Misguich and C. Lhuillier, *Frustrated Spin Systems* (World Scientific, Singapore, 2004).
[4] S.-W. Cheong and M. Mostovoy, Nature (London) **6**, 13 (2007).

[5]R. Moessner and A. Ramirez, Phys. Today **59**, 24 (2006).
[6]A. Ramirez, Nat. Phys. **4**, 442 (2008).
[7]S. Sachdev, Phys. Rev. B **45**, 12377 (1992).
[8]B. Bernu and G. Misguich, Phys. Rev. B **63**, 134409 (2001).
[9]P. Sengupta, A. W. Sandvik, and R. R. P. Singh, Phys. Rev. B **68**, 094423 (2003).
[10]W. Zheng, R. R. P. Singh, R. H. McKenzie, and R. Coldea, Phys. Rev. B **71**, 134422 (2005).
[11]S. Nakatsuji, Y. Nambu, H. Tonomura, O. Sakai, S. Jonas, C. Broholm, H. Tsunetsugu, Y. Qiu, and Y. Maeno, Science **309**, 1697 (2005).
[12]T. Inami, J. Solid State Chem. **180**, 2075 (2007).
[13]S. A. Klimin, M. N. Popova, B. N. Mavrin, P. H. M. van Loosdrecht, L. E. Svistov, A. I. Smirnov, L. A. Prozorova, H.-A. Krug von Nidda, Z. Seidov, A. Loidl, A. Y. Shapiro, and L. N. Demianets, Phys. Rev. B **68**, 174408 (2003).
[14]L. E. Svistov, A. I. Smirnov, L. A. Prozorova, O. A. Petrenko, A. Micheler, N. Buttgen, A. Y. Shapiro, and L. N. Demianets, Phys. Rev. B **74**, 024412 (2006).
[15]K. Hayashi, T. Nozaki, R. Fukatsu, Y. Miyazaki, and T. Kajitani, Phys. Rev. B **80**, 144413 (2009).
[16]D. Grohol and D. Papoutsakis, Angew. Chem. Int. Ed. **40**, 1519 (2001).
[17]D. Nocera, B. Bartlett, D. Grohol, D. Papoutsakis, and M. Shores, Chem. Eur. J. **10**, 3850 (2004).
[18]E. Nytko, M. Shores, J. Helton, and D. Nocera, Inorg. Chem. **48**, 7782 (2009).
[19]W. Geertsma and D. Khomskii, Phys. Rev. B **54**, 3011 (1996).
[20]N. E. Amuneke, D. E. Gheorghe, B. Lorenz, and A. Möller, Inorg. Chem. **50**, 2207 (2011).
[21]A. A. Tsirlin, A. Möller, B. Lorenz, Y. Skourski, and H. Rosner, Phys. Rev. B **85**, 014401 (2012).
[22]R. Nath, A. A. Tsirlin, E. E. Kaul, M. Baenitz, N. Büttgen, C. Geibel, and H. Rosner, Phys. Rev. B **78**, 024418 (2008).
[23]I. Juhász Junger, D. Ihle, L. Bogacz, and W. Janke, Phys. Rev. B **77**, 174411 (2008).
[24]I. Juhász Junger, D. Ihle, and J. Richter, Phys. Rev. B **80**, 064425 (2009).
[25]M. Härtel, J. Richter, D. Ihle, and S.-L. Drechsler, Phys. Rev. B **81**, 174421 (2010).
[26]D. V. Dmitriev, V. Y. Krivnov, and N. Y. Kuzminyh, Phys. Rev. B **84**, 214438 (2011).
[27]L. S. Campana, L. De Cesare, U. Esposito, M. T. Mercaldo, and I. Rabuffo, Phys. Rev. B **82**, 024409 (2010).
[28]J. Rodriguez-Carvajal, *Program* FULLPROF *2000 Vers. 4.80* (Laboratoire Léon Brillouin CEA-CNRS available at http://www.ill.eu/sites/fullprof/, Gif-sur-Yvette, Cedex, France, 2009).
[29]R. Rettich and H. Müller-Buschbaum, Z. Naturforsch. B **53**, 291 (1998).
[30]R. Rettich and H. Müller-Buschbaum, Z. Naturforsch. B **53**, 279 (1998).
[31]Lattice constants from x-ray powder diffraction data refinement (profile fit) at 300 K. However, we limit the standard deviation of the lattice constants to those that are within our experimental setup and refrain from reporting the suggested accuracy of less than 10^{-5} given in the output. For (I) space group $P\bar{3}$, $Z = 1$: $BaAg_2Co[VO_4]_2$ ($a = 5.5310(1)$ Å, $c = 7.1760(1)$ Å, $V = 190.120(3)$ Å^3, $\chi^2 = 1.49$, $R_{\mathrm{Bragg}} = 1.42$, RF factor $= 1.65$); $BaAg_2Ni[VO_4]_2$ ($a = 5.5084(1)$ Å, $c = 7.1481(1)$ Å, $V = 187.834(2)$ Å^3, $\chi^2 = 1.85$, $R_{\mathrm{Bragg}} = 1.71$, RF factor $= 1.90$); $BaAg_2Mg[VO_4]_2$ ($a = 5.5226(1)$ Å, $c = 7.1973(1)$ Å, $V = 190.106(2)$ Å^3, $\chi^2 = 1.55$, $R_{\mathrm{Bragg}} = 1.47$, RF factor $= 1.68$); for (II) space group $C2/c$, $Z = 4$: $SrAg_2Co[VO_4]_2$ ($a = 9.7099(1)$ Å, $b = 5.5645(1)$ Å, $c = 13.7709(2)$ Å, $\beta = 90.443(1)^\circ$, $V = 744.02(2)$ Å^3, $\chi^2 = 2.81$, $R_{\mathrm{Bragg}} = 2.15$, RF factor $= 1.85$); $SrAg_2Ni[VO_4]_2$ ($a = 9.5702(1)$ Å, $b = 5.5295(1)$ Å, $c = 13.7643(1)$ Å, $\beta = 90.094(3)^\circ$, $V = 728.39(1)$ Å^3, $\chi^2 = 3.63$, $R_{\mathrm{Bragg}} = 1.49$, RF factor $= 1.95$); $SrAg_2Mg[VO_4]_2$ ($a = 9.6165(1)$ Å, $b = 5.5418(1)$ Å, $c = 13.7426(1)$ Å, $\beta = 90.316(3)^\circ$, $V = 732.37(2)$ Å^3, $\chi^2 = 1.94$, $R_{\mathrm{Bragg}} = 1.49$, RF factor $= 1.58$).
[32]R. Hoppe, In *Crystal Structure and Chemical Bonding in Inorganic Chemistry* (North-Holland, Amsterdam, 1975), pp. 127–161.
[33]R. Hübenthal, MAPLE, *Vers. 4* (Universität Gießen, 1993).
[34]R. Hoppe, Z. Kristallogr. **150**, 23 (1979).
[35]R. Shannon, Acta Crystallogr. A **32**, 751 (1976).
[36]K. Nakamoto, *Infrared and Raman Spectra of Inorganic and Coordination Compounds* (Wiley Interscience, New York, 2009).
[37]H. Jahn and E. Teller, Proc. R. Soc. London A **161**, 220 (1937).
[38]G. Kortüm, *Reflectance Spectroscopy* (Springer-Verlag, New York, 1969).
[39]B. N. Figgis and M. A. Hitchman, *Ligand Field Theory and Its Applications* (Wiley-VCH, New York, 2000), and references therein.
[40]D. A. Kruse, J. E. Davis, M. Gerloch, J. H. Harding, D. J. Mackey, and R. F. McMeeking, CAMMAG, *a* FORTRAN *computing package* (University Chemical Laboratory, Cambridge, England, 1979).
[41]M. Riley, CAMMAG *for PC, Vers. 4.0* (University of Queensland, St. Lucia, Australia, 1997).
[42]Bonding, Racah and spin-orbit coupling parameters in cm^{-1} used in the calculation. The covalence factor (orbital reduction factor) k_r is dimensionless and was set to 0.8. (I): $e_\sigma = 4250$, $e_\pi = 1250$; (II): $e_{\sigma^1} = 4654$, $e_{\pi^1} = 1369$, $e_{\sigma^2} = 4402$, $e_{\pi^2} = 1295$, $e_{\sigma^3} = 3756$, $e_{\pi^3} = 1105$, note that the differences in interatomic distances M–O(1-3) have been accounted for by deriving the bonding parameters according to a reciprocal power law. For Co^{2+}, $B = 632$, $C = 2658$, $\zeta = 330$ and for Ni^{2+}, $B = 667$, $C = 2934$, $\zeta = 405$ have been used.
[43]M. Bermejo and L. Pueyo, J. Chem. Phys. **78**, 854 (1983).
[44]H. G. Drickamer and C. W. Frank, *Electronic Transitions and the High Pressure Chemistry and Physics of Solids* (Chapman and Hall, London, 1973).
[45]M. E. Lines, Phys. Rev. **131**, 546 (1963).
[46]R. Ray and J. R. Regnard, Phys. Rev. B **9**, 2110 (1974).
[47]L. J. deJong, *Magnetic Properties of Layered Transition Metal Compounds* (Kluver Academic Publishers, Dordrecht, The Netherlands, 1990).
[48]J. P. V. Dyke and W. J. Camp, Phys. Rev. B **9**, 3121 (1974).
[49]W. J. Camp and J. P. V. Dyke, Phys. Rev. B **11**, 2579 (1975).
[50]P. Rabu, S. Angelov, P. Legoll, M. Belaiche, and M. Drillon, Inorg. Chem. **32**, 2463 (1993).
[51]Private communication with A. A. Tsirlin, MPI Dresden: Initial pulsed high-field magnetization measurements at the Dresden High Magnetic Field Laboratory (Helmholtz Zentrum Dresden-Rossendorf) indicate that up to 60 T M(H) increases linear and without reaching the saturation of a $S = 3/2$ system.
[52]Fit proceedure for modifying the specific heat of the Mg compounds to the high-temperature behavior of C_p/T: the zero-field data

of the Mg compounds were calibrated by a factor (f) to the respective maxima of C_p^M/T around 75 K and shifted accordingly in temperature by a value (s). The following adjustments of $C_p^{\mathrm{Mg,M}}/T$ were made for the structure type (I): (Mg,Ni) $f = 0.979$, $s = 3.48$ K; (Mg,Co) $f = 1.026$, $s = 3.48$ K; and for the structure type (II): (Mg,Ni) $f = 0.978$, $s = 1.30$ K; (Mg,Co) $f = 1.068$, $s = 1.45$ K. The low-temperature specific heat data of the original and modified Mg compounds were checked for consistency at very low temperatures, fit of $C_p^{\mathrm{Mg,M}}/T$ versus T^2 ($C_p = \beta_1 T^3$) yields $\beta_1^{\mathrm{Mg,M}}$ in mJ mol^{-1} K^{-4} for type (I): (Mg) 1.92(7), (Mg,Ni) 1.78(8), and (Mg,Co) 1.87(8); and for type (II): (Mg) 1.93(5), (MgNi) 1.53(5), and (Mg,Co) 1.55(6).

[53]L. Onsager, Phys. Rev. **65**, 117 (1944).
[54]N. D. Mermin and H. Wagner, Phys. Rev. Lett. **17**, 1133 (1966).
[55]H. E. Stanly, Phys. Rev. Lett. **20**, 589 (1968).
[56]K. Binder and D. P. Landau, Phys. Rev. B **13**, 1140 (1976).